

Mineralogy-based brittleness prediction from surface seismic data: Application to the Barnett Shale

Roderick Perez Altamar¹ and Kurt Marfurt¹

Abstract

Differentiating brittle and ductile rocks from surface seismic data is the key to efficient well location and completion. Brittleness average estimates based only on elastic parameters are easy to use but require empirical calibration. In contrast, brittleness index (BI) estimates are based on mineralogy laboratory measurements and, indeed, cannot be directly measured from surface seismic data. These two measures correlate reasonably well in the quartz-rich Barnett Shale, but they provide conflicting estimates of brittleness in the calcite-rich Viola, Forestburg, Upper Barnett, and Marble Falls limestone formations. Specifically, the BI accurately predicts limestone formations that form fracture barriers to be ductile, whereas the brittleness average does not. We used elemental capture spectroscopy and elastic logs measured in the same cored well to design a 2D $\lambda\rho-\mu\rho$ to brittleness template. We computed $\lambda\rho$ and $\mu\rho$ volumes through prestack seismic inversion and calibrate the results with the $\lambda\rho-\mu\rho$ template from well logs. We then used microseismic event locations from six wells to calibrate our prediction, showing that most of the microseismic events occur in the brittle regions of the shale, avoiding more ductile shale layers and the ductile limestone fracture barriers. Our $\lambda\rho-\mu\rho$ to brittleness template is empirical and incorporates basin- and perhaps even survey-specific correlations of mineralogy and elastic parameters through sedimentation, oxygenation, and diagenesis. We do not expect this specific template to be universally applicable in other mudstone rock basins; rather, we recommend interpreters generate similar site-specific templates from logs representative of their area, following the proposed workflow.

Introduction

Shales are described as organic-rich, fine-grained reservoirs (Bustin, 2006) and are typically dominated by clays. The mineral composition and the presence of organic matter can influence not only the distribution of pores and fluid saturation (Sondergeld et al., 2010a), but also the effectiveness of stimulation.

Bowker (2003) reports that most of the production in the Barnett Shale comes from zones with 45% quartz content and only 27% clay. In general, the average porosity is 6% with pore throats typically less than 100 nm (Bowker, 2003). Field experiments show that more effective hydraulic fracturing results in improved completion and higher production rates (Saldungaray and Palish, 2012). In the Fort Worth Basin, Gale et al. (2007) describe at least two sets of natural fractures that might be cemented. However, they can be reactivated during hydraulic fracturing, providing a larger rock volume and optimizing production.

Gas is derived from thermogenic cracking of kerogen and from the cracking of any retained oil in the shale (Jarvie, 2003; Montgomery, 2005). Free gas is stored within the rock pores and natural fractures, whereas the adsorbed gas is stored on the organic material.

Although the Barnett Shale formation is capable of generating, retaining, and storing huge amounts of hydrocarbon, gas flow is limited if the individual microreservoir compartments cannot be connected via well stimulation (Jarvie et al., 2007). Hydraulic stimulation connects otherwise unconnected pore spaces.

Analysis to differentiate brittle from ductile rocks has been key to stimulation success in shale gas reservoirs, especially in the Barnett Shale where brittleness is mainly controlled by quartz content. Based on the mineralogy content, ductility (the opposite of brittleness) is controlled by clay, calcite, and total organic content (TOC). Jarvie et al.'s (2007) and Wang and Gale's (2009) brittleness index (BI) defines ductile and brittle regions in terms of its mineralogical content, generating a smooth transition between both regions. In contrast, Grieser and Bray (2007) define an empirical brittleness cut-off based on Poisson's ratio and Young's modulus. The cut-off depends on the shale play in which it is applied and on the expertise of the interpreter.

Perez (2011) combines $\lambda\rho-\mu\rho$ seismic logs with production data to create templates that can be applied to better understand the parameters that control the estimated ultimate recovery (EUR) and stimulated rock

¹ConocoPhillips School of Geology and Geophysics, Norman, Oklahoma, USA. E-mail: roderickperezaltamar@gmail.com; kmarfurt@ou.edu.

Manuscript received by the Editor 10 October 2013; revised manuscript received 8 March 2014; published online 18 August 2014; corrected version published online 20 November 2014. This paper appears in *Interpretation*, Vol. 2, No. 4 (November 2014); p. T255–T271, 13 FIGS., 2 TABLES.

<http://dx.doi.org/10.1190/INT-2013-0161.1>. © 2014 Society of Exploration Geophysicists and American Association of Petroleum Geologists. All rights reserved.

volume in unconventional reservoirs. In the case of stimulated volumes, the templates show the variation in $\lambda\rho-\mu\rho$ for a combination of mineralogical mixtures (quartz and clay) versus total and effective porosity. However, these results do not show a direct link with brittleness.

Brittle rocks are unable to withstand large amounts of strain creating a plane of weakness in the rock, giving rise to microseismic events when they fail. If the rocks are brittle, the injected proppant will keep these fractures open. In contrast, ductile rocks deform plastically and can undergo significant strain prior to fracture. Fractures in more plastic ductile rocks are thought to close about the proppant, thus sealing pathways to fluid flow. Rocks with high brittleness exhibit naturally occurring and hydraulically induced fractures, although in the Barnett Shale, most natural fractures are cemented (Gale et al., 2007).

Brittle rocks may lack natural fractures entirely (Gale et al., 2007) if the loading history is insufficient to drive fracture growth. This is the case most of the time, as documented by lack of fractures or very simple fracture patterns in even highly brittle rocks (Ellis et al., 2012). Subsequently, brittle rocks will only "exhibit" hydraulically induced fractures if a frac job is performed nearby, and in that case, even nonbrittle rocks may fracture. This situation entirely depends on the engineering variables applied, such as completion and treatment techniques, used to hydraulically stimulate the well.

Other authors describe the complexity of the fracture pattern in the Barnett Shale using microseismic event locations and correlate them with seismic attributes to highlight more brittle areas in the formation (Refunjol, 2010; Thompson, 2010, Refunjol et al., 2012). Using the same data set examined in this paper, Thompson (2010) finds that structural ridges are highly cemented, such that most microseismic events occur in bowl-shaped reservoir zones. Simon (2005) finds that microseismic events form a better fracture network in areas that exhibit low-azimuthal velocity anisotropy, resulting in high EUR. In contrast, microseismic events in zones that exhibit higher azimuthal anisotropy produce narrow, elongated fracture patterns, resulting in lower EUR.

The objective in this paper is to predict brittleness from surface seismic data. To do so, we need to reconcile and link conflicting brittleness parameters defined by Grieser and Bray (2007), Jarvie et al. (2007), Rickman et al. (2008), and Wang and Gale (2009).

We begin with a review of the geology and the mineralogy composition of the Marble Falls Limestone, the Upper Barnett Shale, the Forestburg Limestone, the Lower Barnett Shale, and the upper section of the Viola Limestone formations deposited in the Fort Worth Basin, paying special attention to the Barnett Shale formation. Next, we estimate the BI based on the rock mineralogy composition from log measurements in a fully cored well, located just outside the seismic survey. Using density logs and P- and S-wave sonic logs in the well, we

calculated Young's modulus, Poisson's ratio, $\lambda\rho$, and $\mu\rho$. Then, we proceed to map these variables against the BI, and we use this template to predict brittleness from surface seismic inversion, which were calibrated and analyzed using microseismic event locations.

The Barnett Shale

"The Fort Worth Basin is a shallow north-south elongated foreland basin, encompassing roughly 15,000 mi² in North Texas, formed during the late Paleozoic Ouachita Orogeny" (Walper, 1982). Paleotectonic collision events in the Fort Worth Basin resulted in a northwest-southeast main stress field orientation at the time of the Barnett Shale deposition. However, the present-day regional maximum stress direction in the basin is northeast-southwest, with local deviations in intensity and direction about the mineral wells and other minor faults (e.g., Simon, 2005).

The Barnett Shale is an organically rich and thermally mature rock deposited during Mississippian time (≈ 340 Ma) in the Fort Worth Basin, characterized by low average permeability (70 nD) and porosity (6%) distributed in a variety of depositional facies (Deacon, 2011). The Viola, Forestburg, and Marble Falls Limestones are hydraulic fracture barriers and are not considered production targets because they are water-bearing. The Viola Formation deposited on top of the karsted Ellenburger Formation (Loucks, 2008) presents a potential risk of water production. In the area of study, the Forestburg Limestone divides the Upper Barnett and the Lower Barnett shales into two members, which must be treated and fractured separately.

Singh (2008) and Perez (2009) describe three distinctive gamma ray (GR) log patterns: upward-increasing, upward-decreasing, and constant. These GR log patterns are correlated to lithofacies using cored wells in the Barnett Shale representing unique deposition environments. Singh (2008) defines the upward-increasing GR parasequence (GRP) to be composed of upward-increasing amounts of clay accompanied by a decrease in calcite content.

Kale (2009) and Gao (2011) combine Singh's (2008) 10 petrofacies into three petrotypes exhibiting similar petrophysical properties. Kale (2009) bases his classification on porosity, TOC, and total carbonate measurements. These petrotypes are then ranked in terms of cumulative production data from three vertically cored wells.

Mineralogy

Conventional logs such as GR, neutron porosity, and resistivity are useful to stratigraphically characterize a reservoir. However, these logs do not fully provide the information needed to characterize organic shales in terms of their geomechanical behavior. This additional information can come from the integration of sequence stratigraphy, special analysis techniques, specialized logging tools, and core lab measurements. Recent availability of mineralogy logs such as elemental

capture spectroscopy (ECS) and dipole sonic logs enable characterization of a reservoir in terms of its mineral content and elastic properties, providing a means to differentiate lithology types by their completion response.

Core and outcrop studies show the Barnett Shale to be dominated by clay- and silt-size sediment with occasional beds of skeletal debris. Organic and biogenic constituents were deposited at the time of the sedimentation of the Barnett Shale and include algal remains, spores, plant remains, sponges, and radiolarians, among others (Slatt, 2011). After sedimentation, chemical reactions lead to the generation of secondary minerals including authigenic clays, calcite, dolomite, quartz, pyrite, and hydrothermal minerals (Slatt and O'Brien, 2011).

Based on several wells, Jarvie (2003) reports that the mean composition of the Barnett Shale in the region consists of 40% quartz, 29% illite (with minor smectite), 13% calcite, 3% organic matter, and 2% pyrite. Karastathis (2007) reports that the Upper Barnett Shale shows a higher carbonate content than the Lower Barnett Shale, with the main carbonate minerals present in the formation being calcite, dolomite, siderite, and aragonite with calcite being dominant. Illite is the dominant clay mineral, contributing close to 70% by weight to the overall clay content (Kale, 2009).

In addition to conventional logs, ECS logs were also acquired in the area of the study, revealing important vertical and lateral mineralogy variations. The ECS technique measures relative elemental yield based on neutron-induced capture GR spectroscopy, detecting silicon (Si), iron (Fe), calcium (Ca), sulfur (S), titanium (Ti), gadolinium (Gd), chlorine (Cl), barium (Ba), and hydrogen (H), but not magnesium (Mg). The ECS tool sends neutrons into the wellbore wall, while a detector measures the counts and energy spectrum from the released GRs. The algorithm combines the resulting spectrum with other logs such as the bulk density and photoelectric factor, among others, to interpret the most likely mineralogy composition of the rock.

In our study, the ECS results have been calibrated with several cored wells in the area. Figure 1 shows the mineralogy ternary plot corresponding to a representative well in the area of study where the sum of all the clay, quartz, and calcite minerals is displayed on each individual vertex of the ternary plot, indicating that the mineral distribution along the wellbore agrees with Karastathis' (2007) and Kale's (2009) previous findings. Other authors (Sondergeld et al., 2010b; Slatt, 2011) have used similar mineralogy log tools to characterize shale reservoirs. Table 1 summarizes the mean weight mineralogy composition of the main formations computed from ECS data corresponding to seven wells in the area of study. The ECS data indicate that the Lower Barnett Shale has higher quartz content than the Upper Barnett Shale, agreeing with core measurements made by Kale (2009) and Karastathis (2007).

Conventional log sets such as GR (Figure 2, track 2), photoelectric factor, and resistivity were acquired in the area, and they differentiate shale from limestone formations. Applying the same concept used by Singh (2008) and Perez (2009), we interpret the GR log pattern (indicated by arrows in Figure 2, track 2) and their corresponding GRP (Figure 2, track 3).

Organic-rich sediments (source rock) that contain significant amounts of organic matter have a higher resistivity and sonic transit time than organic-lean sediments. Also, organic-rich rocks are often highly radioactive, which is easily seen on GR log measurements (Schmoker, 1981a, 1981b). The TOC in this paper was calculated using a Schlumberger proprietary methodology, which has been calibrated by hundreds of TOC core data from other wells in the basin. TOC varies between 1% and 11% as shown on track 8 in Figure 2, and it agrees with TOC core measurements from Singh (2008).

Brittleness

When a rock is subjected to increasing stress, it passes through three successive stages of deformation: elastic, ductile, and fracture. Based on these behaviors, it is possible to classify the rocks into two classes: ductile and brittle. If the rock has a smaller region of elastic behavior and a larger region of ductile behavior, absorbing much energy before failure, it is considered ductile. In contrast, if the material under stress has a larger region of elastic behavior but only a smaller region of ductile behavior, the rock is considered brittle.

The measurement of stored energy before failure is known as brittleness, and it is a complex function of rock strength, lithology, texture, effective stress, temperature, fluid type (Handin and Hager, 1957, 1958; Handin et al., 1963; Davis and Reynolds, 1996), diagenesis, and TOC (Wells, 2004). Brittleness is defined by

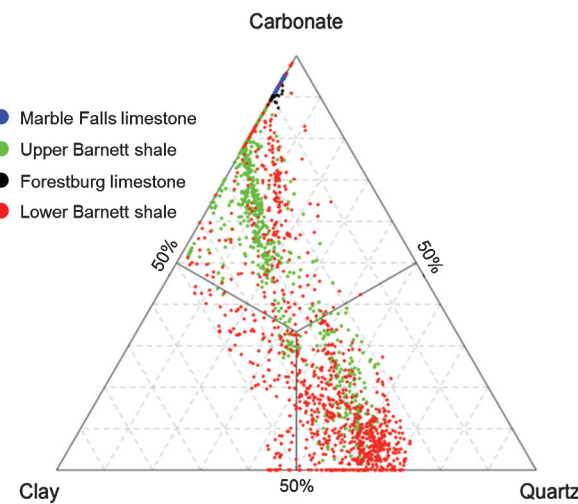


Figure 1. A representative ternary mineralogy distribution plot of quartz, carbonate, and clay for the Marble Falls Limestone, Upper Barnett Shale, Forestburg Limestone, and the Lower Barnett Shale from ECS log measurements corresponding to well A (the well location is shown in Figure 10c).

researchers for different purposes. Hetenyi (1966) defines brittleness as *the lack of ductility*. Ramsey (1967) states that when the internal cohesion of rocks is broken, the rocks are said to be brittle. Obert and Duvall (1967) define brittleness as *a property of materials that rupture or fracture with little or no plastic flow*.

Several of the more commonly used brittleness definitions neglect geologic factors such as the rock com-

position and the origin and habit of mineral rock components (such as quartz and calcite, and/or the type of cement in the rock). To estimate a reliable and robust reservoir brittleness measurement, it is necessary therefore to combine conventional well logs with direct measurements of geomechanical properties, such as Young's modulus E and Poisson's ratio ν (Grieser and Bray, 2007; Rickman et al., 2008).

Table 1. Fractional mean weight mineralogy composition of the formations from seven elemental capture spectroscopy well logs in the area of study, where MF Lm corresponds to the Marble Falls Limestone, UB Sh to the Upper Barnett Shale, F Lm to the Forestburg Limestone, LB Sh to the Lower Barnett Shale, and V Lm to the Viola Limestone Formations.

Formation	Quartz wgt. (%)	Pyrite wgt. (%)	Illite wgt. (%)	Calcite wgt. (%)	Dolomite wgt. (%)	Clay wgt. (%)	TOC wgt. (%)
MF Lm	0.000	0.000	0.067	0.925	0.000	0.064	0.000
UB Sh	0.142	0.007	0.148	0.334	0.000	0.219	0.150
F Lm	0.001	0.000	0.065	0.844	0.000	0.090	0.000
LB Sh	0.339	0.016	0.189	0.116	0.000	0.229	0.111
V Lm	0.016	0.000	0.044	0.886	0.000	0.054	0.000

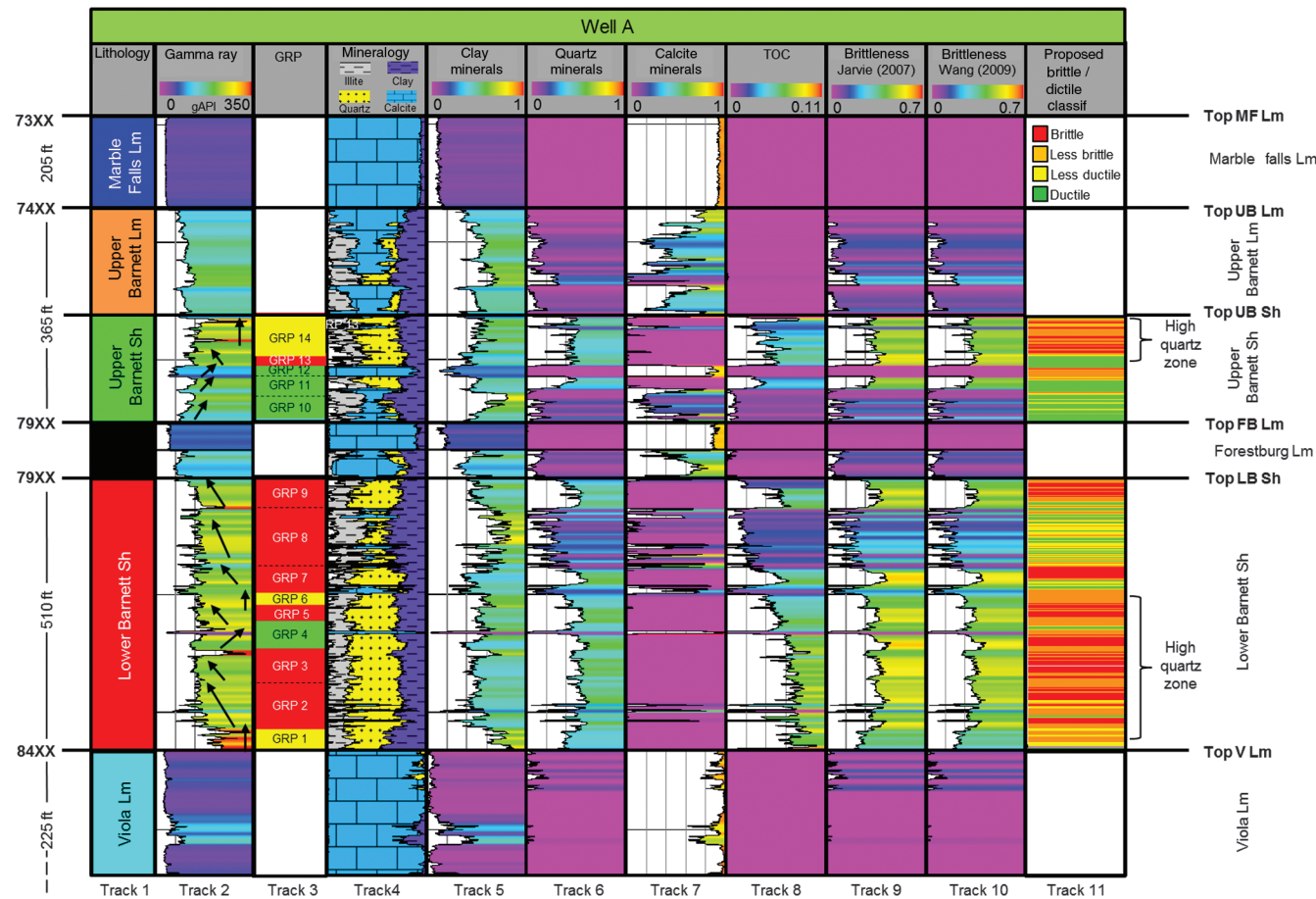


Figure 2. GR, GRPs, and mineralogy logs corresponding to well A (tracks 1, 2, and 3, respectively). Track 4 shows the ECS log corresponding to well A indicating that the mineral distribution along the wellbore agrees with Karastathis' (2007) and Kale's (2009) findings, whereas tracks 5, 6, and 7 show the individual mineralogy log results decomposed into clay, quartz, and calcite mineral content, respectively. The BI logs are calculated using Jarvie et al. (2007) (track 9) and Wang and Gale (2009) (track 10). Track 11 shows the classification results from Figure 3d, where brittle (red) and more brittle zones (orange) are associated with high quartz and TOC content zones.

The brittleness index

The BI is a relative measurement that depends on the field of study and the purpose of the investigation (Altindag and Guney, 2010). One common BI measure is the ratio of compressive strength σ_c to tensile strength σ_t (Coates and Parsons, 1966; Aubertin and Gill, 1988; Baron, 1992; Aubertin et al., 1994; Ribacchi, 2000; Ha-jiabdolmajid and Kaiser, 2003):

$$BI = \frac{\sigma_c}{\sigma_t}. \quad (1)$$

Because tensile strength and compressive strength are measured only in the laboratory, it is difficult to extend this definition to the reservoir scale. The higher the magnitude of the BI, the more brittle the rock.

Jarvie et al. (2007) and Wang and Gale (2009) propose BI definitions based on the mineral composition of the rock, dividing the most brittle minerals by the sum of the constituent minerals in the rock sample, considering quartz (and dolomite, in the case of Wang and Gale, 2009) as the more brittle minerals:

$$BI_{\text{Jarvie}(2007)} = \frac{Qz}{Qz + Ca + Cly}, \quad (2)$$

and

$$BI_{\text{Wang}(2009)} = \frac{Qz + Dol}{Qz + Dol + Ca + Cly + TOC}, \quad (3)$$

where Qz is the fractional quartz content, Dol is the dolomite content, Ca is the calcite content, TOC is the to-

tal organic carbon content, and Cly is the clay content by weight in the rock.

Jarvie et al.'s (2007) equation 2 estimates BI using quartz in the numerator, and the sum of quartz, clay, and calcite in the denominator. In contrast, Wang and Gale's (2009) equation 3 extends this formulation by including dolomite as a contributor to brittleness in the numerator, and TOC and dolomite in the sum of constituent minerals of the rock in the denominator.

We calculate the BI using Jarvie et al.'s (2007) and Wang and Gale's (2009) equations using the ECS log data points and show the results in Figure 2, tracks 9 and 10, respectively. Comparing both BI indices with the mineralogy logs (Figure 2 track 4), we observe that the zones with high quartz and calcite content are more brittle than the regions with high clay content, which are less brittle (ductile).

In the absence of dolomite (Table 1), Jarvie et al.'s (2007) and Wang and Gale's (2009) BI results differ subtly because Wang and Gale (2009) includes TOC in the equation, increasing the ductility of the rock. Because TOC in some zones is close to 10% (wgt.), we will use Wang and Gale's (2009) equation in the remaining analyses.

We crossplot GR versus BI for all the formations in Figure 3a, showing that the shale formations (Upper and Lower Barnett Shale) exhibit moderate to high-GR and BI values. Exceptionally high-GR values (>200 API) correspond to thin layers containing highly radioactive phosphatic nodules and concretions (Singh, 2008). Counterintuitively, this crossplot shows a positive correlation between GR and BI. As expected, limestone formations (Marble Falls Limestone, Forestburg

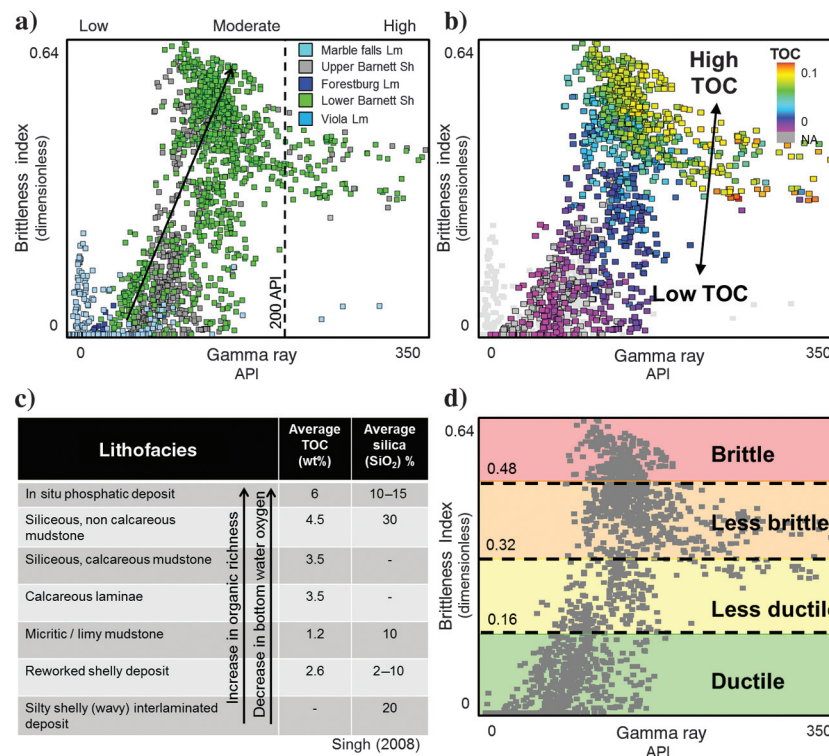


Figure 3. (a) GR versus BI corresponding to well A (using Wang and Gale's [2009] equation) differentiating the Marble Falls Limestone (cyan), Upper Barnett Shale (gray), Forestburg Limestone (dark blue), Lower Barnett Shale (green), and Viola (blue). (b) GR versus BI corresponding to the Upper and Lower Barnett Shale color coded by TOC content, and (c) Singh (2008) Barnett Shale lithofacies definition ranked in relation to interpreted relative bottom oxygenation and organic richness. (d) Brittle (red), less brittle (orange), less ductile (yellow), and ductile (green) classification proposed (classification results are shown in track 12 in Figure 2).

Limestone, and Viola Limestone) show low-GR and low-BI values. Notice that the Viola Limestone formation (light blue) exhibits a subtle positive variation in BI related to clay content in the limestone formation.

Color-coding the previous crossplot with TOC content reveals that high TOC values correspond to high brittleness and high-GR values (Figure 3b), conflicting with equation 3. It is important to highlight that TOC is a direct measurement of organic richness, and its preservation depends on the bottom oxygen levels at the time of deposition (Singh, 2008). Oxygenated strata are characterized by bioturbation and benthic activity, which can be responsible for lowering the TOC. Based on this, Singh (2008) defines a relationship between the position of the described lithofacies in relation to the rela-

tive bottom oxygenation and its organic richness. She concludes that the phosphatic, siliceous noncalcareous mudstone, and siliceous calcareous mudstone lithofacies exhibit higher TOC, in contrast to the silty shale and reworked shelly deposits, which exhibit lower TOC (Figure 3c). Based on these depositional constraints TOC and quartz are correlated such that high-TOC zones are more brittle in our study area.

In Figure 3d, we break the data population into four equal petrotypes, setting the BI between 0 and 0.16 as ductile (green), between 0.16 and 0.32 as less ductile (yellow), between 0.32 and 0.48 as less brittle (orange), and greater than 0.48 as brittle (red). We plot the classification results on track 11 on Figure 2. Examining the GR log along with the ductile/brittle classification

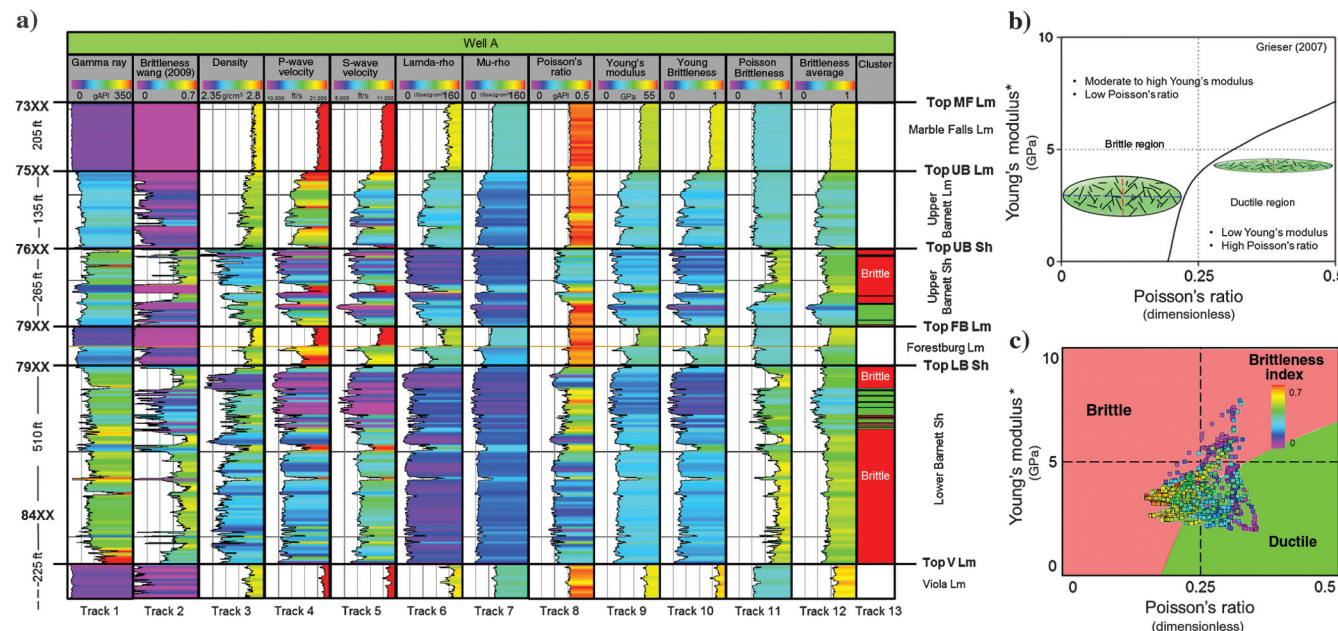


Figure 4. (a) Set of elastic logs corresponding to well A, (b) Poisson's ratio versus Young's modulus crossplot indicating empirically defined ductile-brittle regions, and the expected fracture pathway geometry (modified from Grieser and Bray, 2007), (c) the Poisson's ratio versus Young's modulus values corresponding to formations in well A overplotted by Grieser and Bray's (2007) ductile (green)-brittle (red) regions color coded with BI from ECS mineralogy analysis. Classification results are shown in track 13 in panel (a).

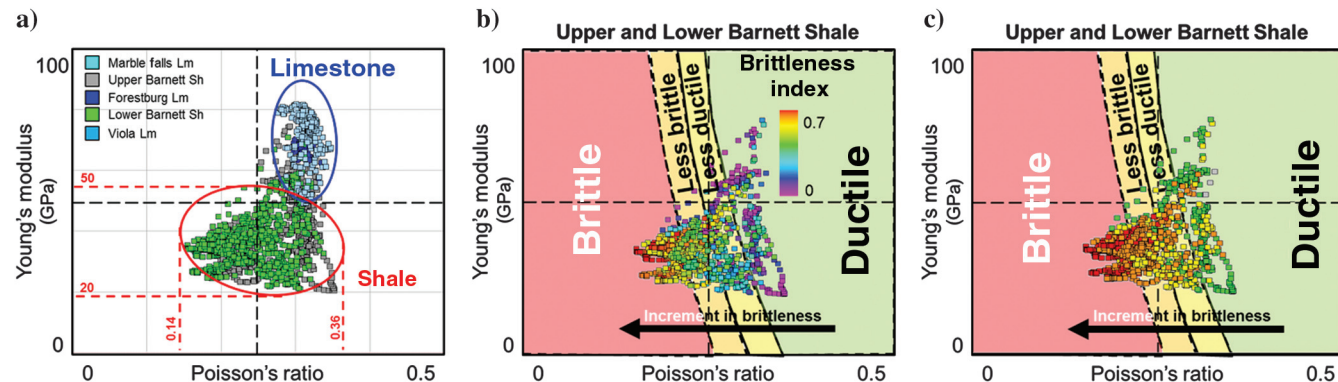


Figure 5. (a) Poisson's ratio versus Young's modulus crossplot corresponding to each formation in the study area. (b) Poisson's ratio versus Young's modulus crossplot corresponding to Upper and Lower Barnett Shale color coded by BI, overlapped by a proposed brittle/ductile classification and (c) the proposed classification.

results based on BI, we observe that the mid-lower part of the Lower Barnett Shale and the middle section of the Upper Barnett are the more brittle zones because of their higher quartz content in the vertical section. Also, we identify from the log several thin ductile layers (green) within the shale formation related to high clay mineral content.

The brittleness average

The term brittleness average is proposed by Grieser and Bray (2007) as an empirical relationship between Poisson's ratio and Young's modulus to differentiate ductile from brittle regions. They hypothesize that ductile rocks exhibit a low Young's modulus and high Poisson's ratio, whereas brittle rocks exhibit a moderate to high Young's modulus and low Poisson's ratio. Grieser and Bray (2007) normalize Young's modulus and Poisson's ratio by their ranges, resulting in scaled elastic parameters:

$$E_{\text{brittleness}} = \frac{E - E_{\min}}{E_{\max} - E_{\min}}, \quad (4)$$

where E is Young's modulus, and E_{\min} and E_{\max} are the minimum and maximum Young's modulus measured in the logged formation, and

$$\nu_{\text{brittleness}} = \frac{\nu - \nu_{\max}}{\nu_{\min} - \nu_{\max}}, \quad (5)$$

where ν is Poisson's ratio, and ν_{\max} and ν_{\min} are the maximum and minimum values of Poisson's ratio logged in the formation.

Finally, they define a brittleness average, BA, as

$$\text{BA} = \frac{E_{\text{brittleness}} + \nu_{\text{brittleness}}}{2}. \quad (6)$$

We use the elastic logs corresponding to well A (Figure 4a) to compute Poisson's ratio and Young's modulus logs and display the results on tracks 8 and 9 in Figure 4a. We calculate Young's modulus brittleness and Poisson's ratio brittleness using equations 4 and 5 and display the results on tracks 10 and 11 in Figure 4a. Finally, we calculate the brittleness average (using equation 6) and display the results on track 12 in

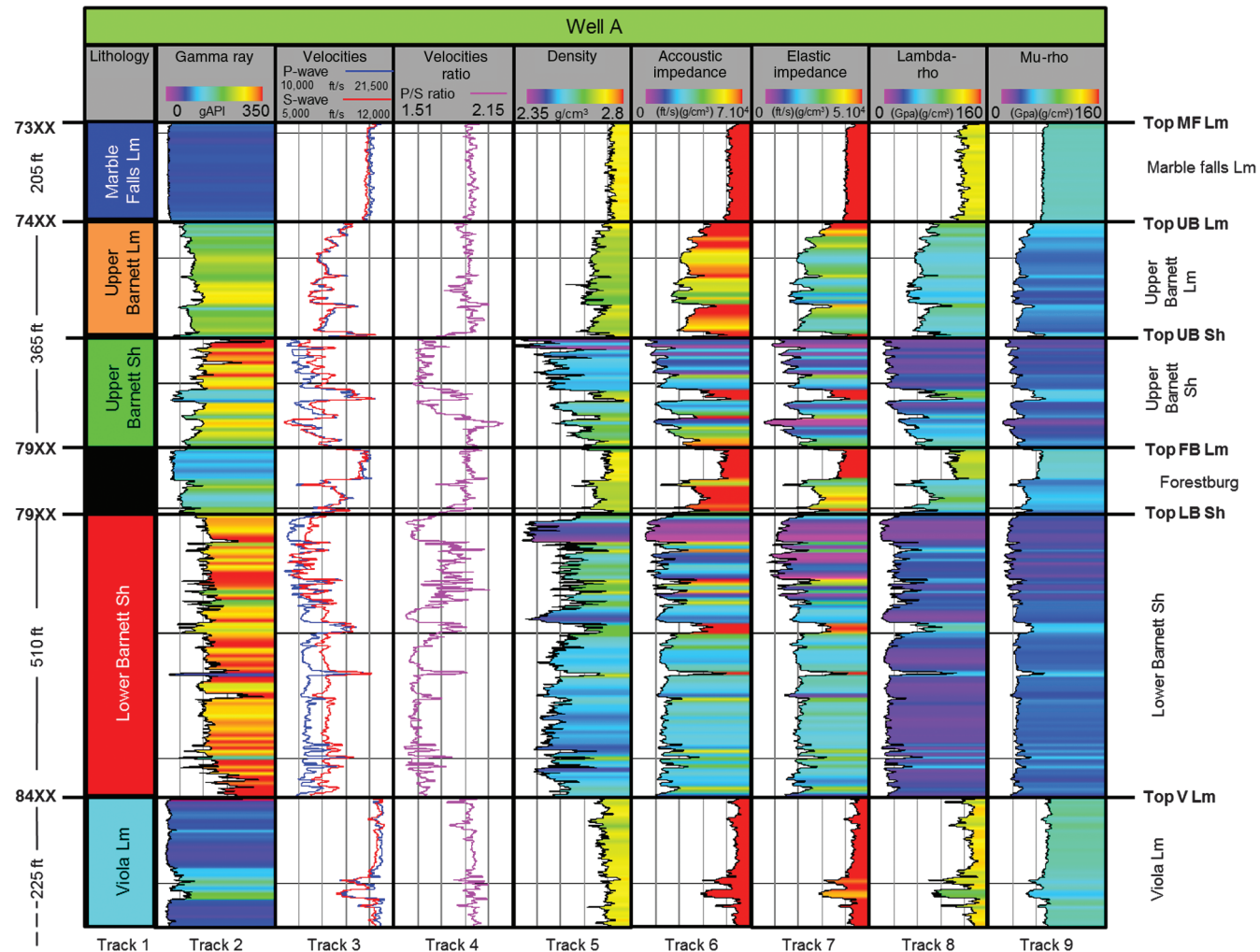


Figure 6. GR, V_p , V_s , velocity ratio, and density logs corresponding to the same representative well, and its acoustic and elastic impedance $\lambda\rho$ and $\mu\rho$ logs.

Table 2. The $\lambda\rho$ and $\mu\rho$ values of the three most common minerals in the Barnett Shale (calcite, clay, and quartz) using the moduli, densities, and velocities published by Mavko et al. (2009).

Mineral	$\lambda\rho$ (GPa) (g/cm ³)	$\mu\rho$ (GPa) (g/cm ³)
Quartz	20.32	116.60
Clay	48.45	22.95
Calcite	149.41	88.08

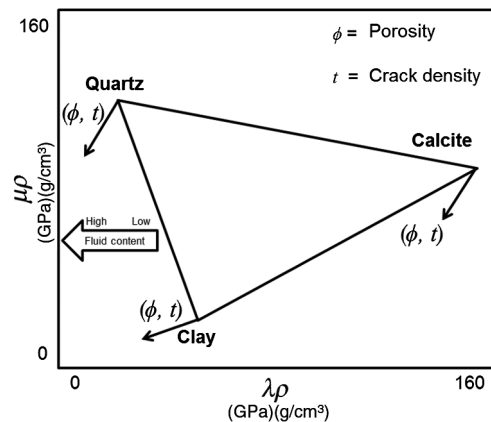


Figure 7. The $\lambda\rho$ - $\mu\rho$ values corresponding to solid pure minerals of quartz, calcite, and clay are calculated using rock laboratory measurements published by Mavko et al. (2009). Arrows represent the expected change of $\lambda\rho$ and $\mu\rho$ with increasing porosity (ϕ), fluid content, and crack density (t).

Figure 8. The $\lambda\rho$ - $\mu\rho$ crossplot (a) color coded by GR, (b) color coded by TOC, (c) color coded by BI (extracted from mineralogy) overplotted by a proposed brittle/ductile classification, and (d) the proposed BI classification.

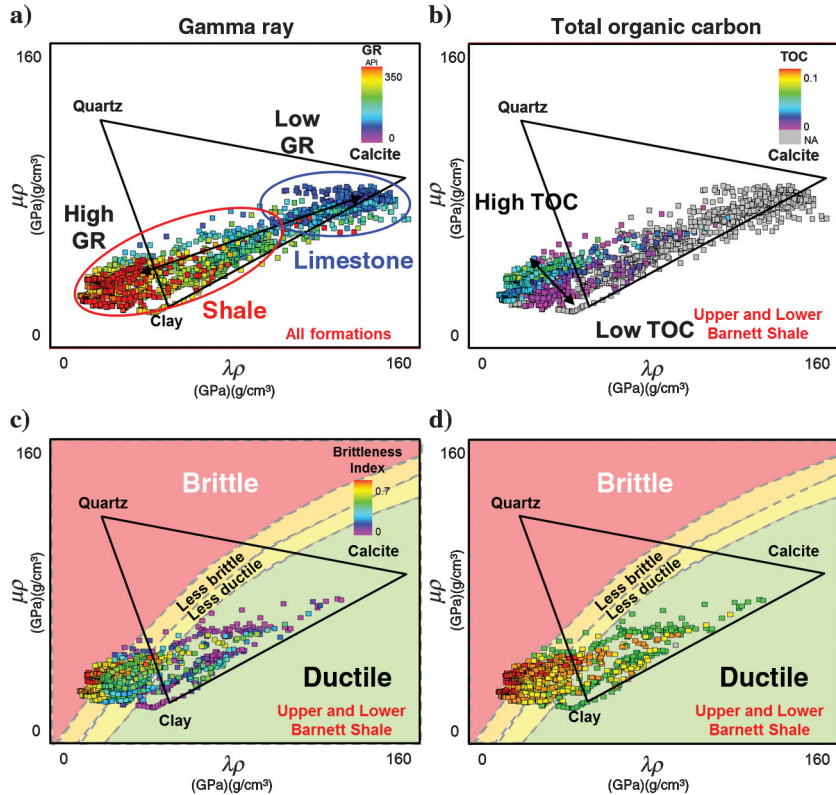


Figure 4a. Notice the differences in brittleness average in the formations, showing that the lower section is more brittle than the upper section of the Lower Barnett Shale, and the upper section of the Upper Barnett Shale is more brittle than the lower section. The brittleness average (track 12 in Figure 4a) is somewhat smoother than the BI (track 2 in Figure 4a) because the ECS log tool has a finer resolution (≈ 1.5 ft) than the sonic and dipole sonic log (≈ 3 ft).

Poisson's ratio versus Young's modulus brittleness crossplots

Crossplotting Poisson's ratio versus Young's modulus, the shales with low average BI values fall into the ductile (green) region proposed by Grieser and Bray (2007) (Figure 4b). Using this template, we plot Poisson's ratio and Young's modulus corresponding to all the formations corresponding to well A, color coded using the BI calculated previously. Shales with high BI fall into the brittle region (red) agreeing with Grieser and Bray's (2007) definition. We plot the classification results in track 13 in Figure 4a. Notice that a cloud of low-BI (ductile) points (color coded in purple) falls into the brittle region, generating a conflict. To clarify these conflicting results, we classify the shale and limestone formations in terms of its Poisson's ratio and Young's modulus in Figure 5a. The Upper and Lower Barnett Shale exhibit Poisson's ratio ranging from 0.14 to 0.36 and Young's modulus from 20 to 50 GPa.

Wang and Gale's (2009) BI definition assumes that quartz and dolomite are the most brittle minerals in

the rock. Those rocks with low negligible amounts of these two minerals, such as limestone or shaly limestones, will be considered to be ductile. Limestone formations are not a completion target in this study. They do not have hydrocarbon potential but rather serve as a frac barrier. For these reasons, they are displayed in white in Figure 4a, track 13. Although Grieser and Bray's (2007) crossplot is useful in the absence of mineralogy logs, it fails to differentiate between brittle quartz-rich shales and ductile limestones. Given the transition between shale and limestone through the Upper Barnett Limestone, the direct use of the template shown in Figure 4b is problematic.

The $\lambda\rho$ versus $\mu\rho$ brittleness crossplots

Goodway et al. (1997) demonstrate that it is possible to extract lithology and pore fluid information from $\lambda\rho$ to $\mu\rho$ crossplots derived from surface seismic and well logs. Goodway et al. (1997) and Perez (2011)

present $\lambda\rho$ - $\mu\rho$ lithology templates, which have been very useful for reservoir characterization and correlating brittleness to rock properties. Goodway et al. (2010) use these templates to estimate the minimum closure stress from seismic estimates of $\lambda\rho$ and $\mu\rho$.

P-wave sonic, dipole sonic, and density logs were used to calculate acoustic impedance, elastic impedance, $\lambda\rho$, and $\mu\rho$ logs corresponding to well A (Figure 6). We also compute and plot the $\lambda\rho$ and $\mu\rho$ of the three most common minerals in the Barnett Shale: calcite, clay, and quartz (Table 2, see Figure 7) using the moduli, densities, and velocities published by Mavko et al. (2009). Connecting the three vertices of each mineral generates a mineralogy ternary plot in the $\lambda\rho$ - $\mu\rho$ space (Figure 7). These calculations assume zero porosity ($\phi = 0$); introducing cracks and pores is nontrivial and is left for future investigation. As porosity (ϕ), fluid content, and crack density (t) increase, the results will mimic a triangular form but the values will be shifted

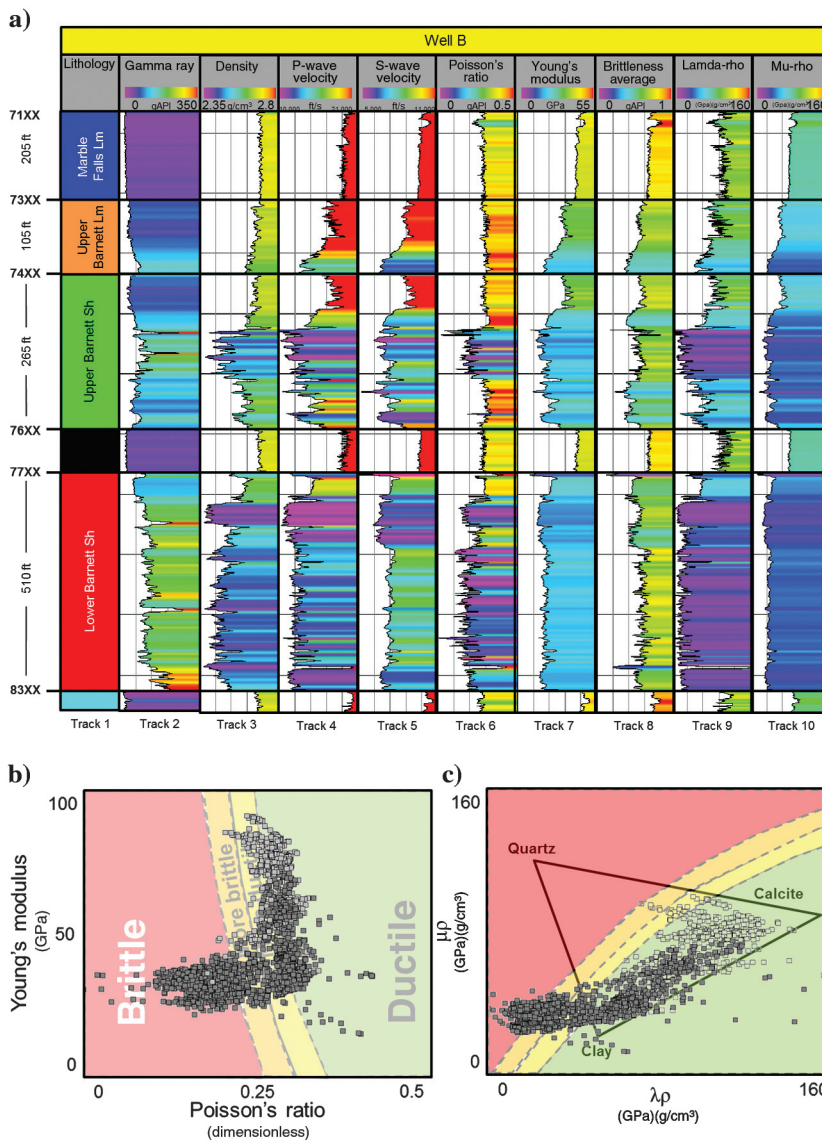


Figure 9. (a) GR, density, V_p , and V_s logs corresponding to well B (the well location is shown in Figure 10c), its corresponding (b) Poisson's ratio versus Young's modulus crossplot, and (c) $\lambda\rho$ - $\mu\rho$ crossplot overlapped by the proposed brittle/ductile template.

horizontally along the x -axes as lines of constant $\mu\rho$. This shift is caused by the gas saturation effects that decrease the values of $\lambda\rho$ toward the origin (Goodway et al., 2006). Berryman et al. (1999, 2002) report similar results and created several $\lambda\rho$ - $\mu\rho$ crossplots discriminating porosity and saturation effects. We expect that the lateral displacement rate is not the same between clastic and carbonate rocks. Usually, clastic rocks have a higher crack density than carbonates; in contrast, cracks in carbonates tend to be wider and larger.

Using the $\lambda\rho$ - $\mu\rho$ template described previously for the three most common minerals in the area of study as a reference, the $\lambda\rho$ - $\mu\rho$ well log results were cross-plotted and color coded by the GR values, resulting in high-GR regions (shale) and low-GR values (limestone) (Figure 8a). As discussed previously, high-TOC zones (Figure 8b) are depositionally related to high quartz content and to high BI. We will use the template in Figure 8c to predict BI from $\lambda\rho$ - $\mu\rho$ estimates made from surface seismic data.

Because well A is located out of the seismic survey area, the same workflow discussed previously is repeated for well B. The corresponding well log results are shown in Figure 9a. An ECS well log is not available in well B. We therefore use the same brittle-ductile regions in the $\lambda\rho$ - $\mu\rho$ defined from well A in Figure 9b and 9c.

Brittleness prediction and calibration

High-quality long-offset surface seismic data were acquired after more than 400 wells were drilled and completed in the area of study. Using commercial software, we simultaneously inverted the data to estimate $\lambda\rho$ and $\mu\rho$ following the workflow presented by Goodway et al. (1997).

Microseismic mapping is a passive seismic technique that records events generated as a consequence of processes within the reservoir such as fluid flow and hydraulic fracturing (McGillivray, 2005; Daugherty and Urbancic, 2009; Noe, 2011). Microseismic data are used to map fracture growth (Waters et al., 2009) and have been useful in mapping the effectiveness of the hydraulic fracturing job (e.g., Simon, 2005). Typical microseismic data products include the approximate coordinates in space, local time of occurrence, and magnitude of each event. Using microseismic events Refunjol et al. (2012) find that fracture-prone rocks are consistently characterized by a specific range of P- and S-impedance, suggesting that properties extracted from surface seismic properties can be useful in highlighting zones where the rock is prone to failure during hydraulic stimulation.

Event locations corresponding to wells C and D are shown in Figure 10a and 10b, respectively. The

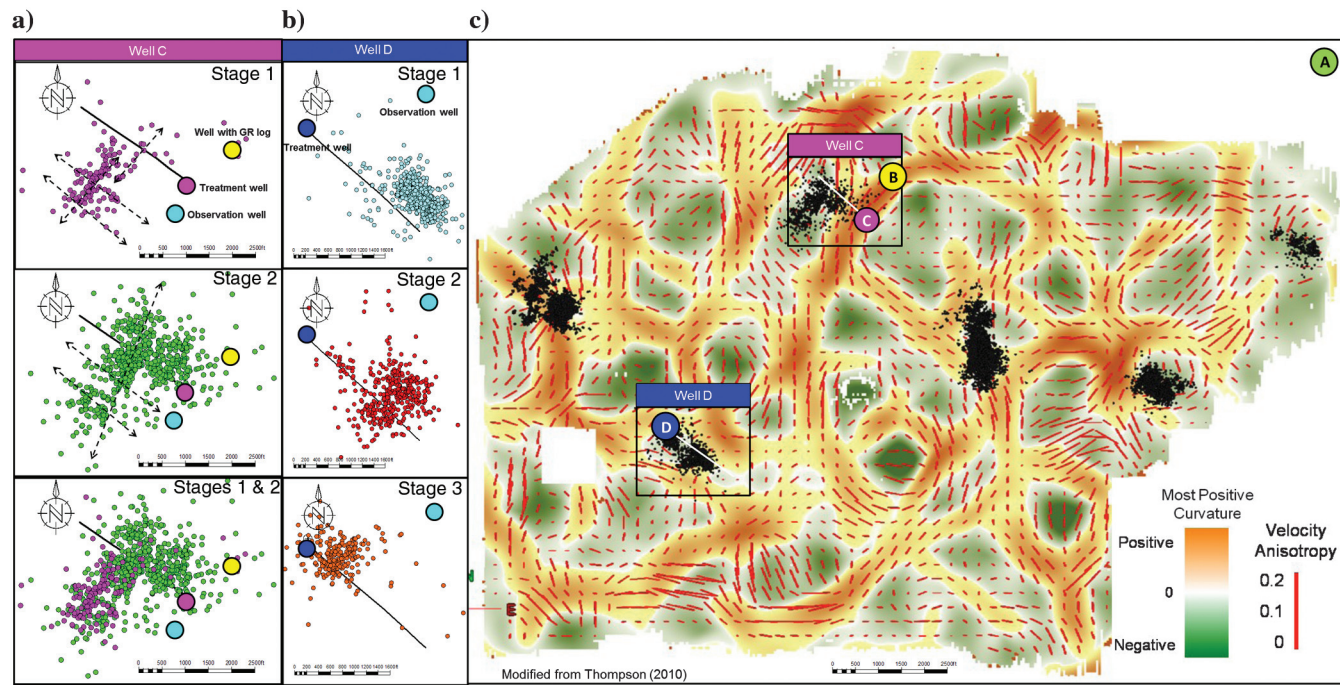


Figure 10. Map view of microseismic event locations corresponding to (a) well C and (b) well D; the orientation of the fracture lineaments formed by the microseismic events align with the current maximum horizontal stress direction in the Fort Worth Basin (northeast–southwest). (c) Horizon slice along the top Viola Limestone through the most positive curvature seismic attribute volume. Most of the microseismic event locations fall into the areas with negative curvature values (bowl shapes). Red vectors indicate velocity anisotropy in which the length of the vector is proportional of the degree of anisotropy, and the direction indicates the azimuth of maximum anisotropy (modified from Thompson, 2010). The seismic data were acquired after 400 wells were stimulated, such that the velocity anisotropy represents the postfrac stress regime. The location the cored and ECS shown in Figure 2 is indicated as well A, northeast of this seismic survey.

hydraulic fracture job started at the toe and ended at the heel of each well. In both cases, the map view shows that some of the events preferentially aligned (dashed lines) with the current northeast–southwest maximum horizontal stress in the Fort Worth Basin (Heidbach et al., 2009).

In the case of well C, most of the microseismic events extend to the southwest of the well at stage 1, in contrast to stage 2, in which the events are more centered about the wellbore. For stage 1 in well D, most of the events are northeast of the wellbore. Notice from Figure 10c that microseismic events corresponding to well C and well D trend toward negative values of the most positive curvature (green) indicating bowls, avoiding the positive values (orange) indicating ridges and domes, exhibiting the same behavior described by Browning (2006) and Thompson (2010). Browning (2006) observes that microseismic event locations occur more often in negative curvature zones, whether the well was drilled onto a

positive or into a negative curvature zone. Because the seismic survey was acquired after the reservoir was intensively fractured, we interpret the velocity anisotropy seen in Figure 10c to be correlated to the open induced fracture network (H. Lynn, personal communication, 2010). Zhang (2010) finds the azimuthal anisotropy to be highly variable, but locally organized.

Figure 11a shows the lateral view of microseismic events about well C, while Figure 11b shows the depth histograms at each stage revealing that most of the events are concentrated in the Lower Barnett Shale, close to the wellbore. More microseismic events are recorded in stage 2 than in stage 1. Stage 2 may have been influenced by the fractures generated by stage 1. The previous map view (Figure 10a) reveals that the event locations corresponding to stage 1 are confined into a smaller region than those from stage 2.

In addition to mineralogy and elastic parameters, there are other parameters that can affect brittleness,

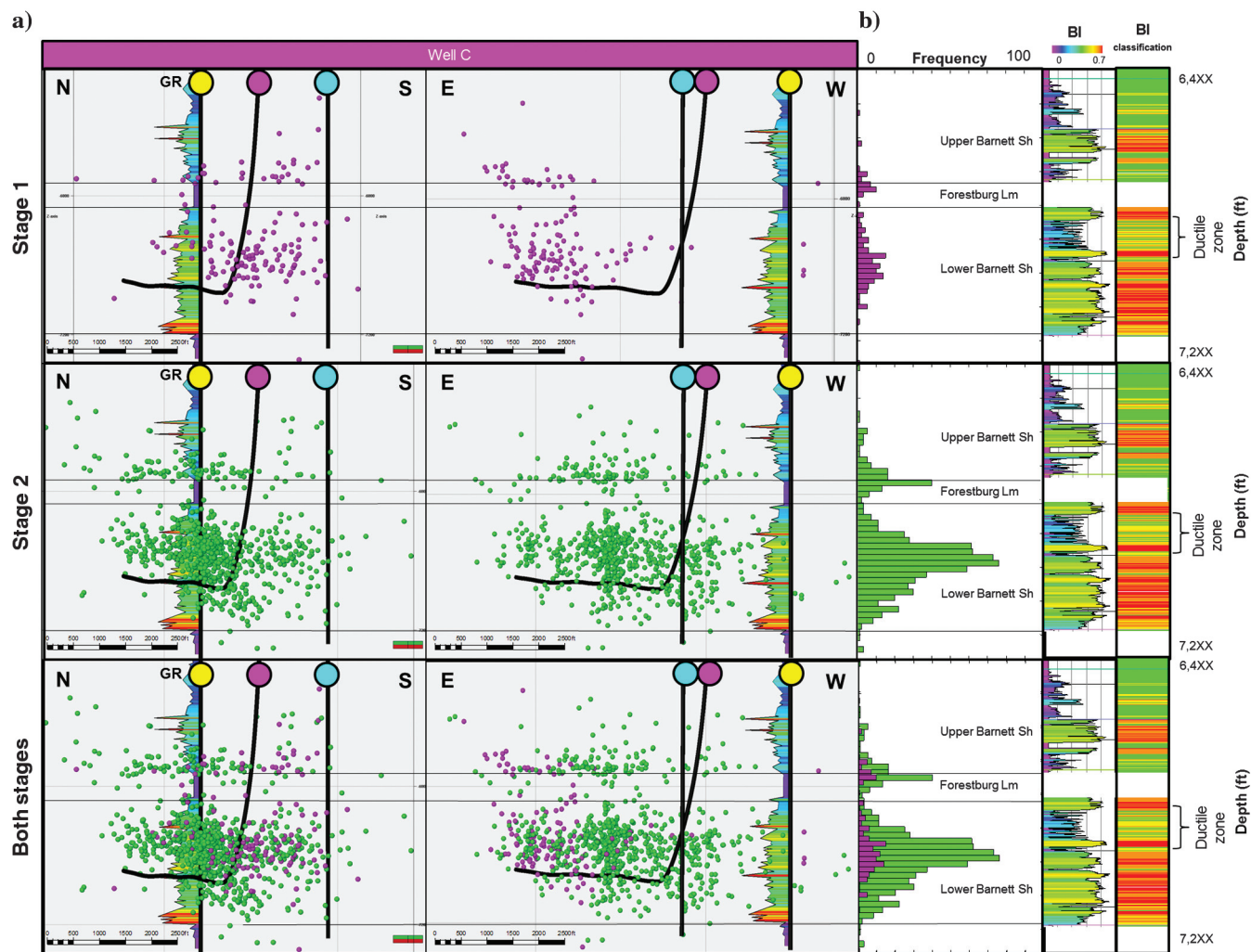


Figure 11. (a) Lateral view and (b) microseismic vertical (depth) histograms, GR, BI log, and BI classification (brittle [red], less brittle [orange], less ductile [yellow], and ductile [green]) corresponding to individual stages of microseismic event locations corresponding to well C. Vertical histogram shows a decrease in events recorded in the upper section of the Lower Barnett Shale toward the Forestburg Limestone, possibly due to the increment in clay minerals and therefore ductility, creating a ductile zone.

such as the degree of interbedding (Sierra et al., 2010) and the scale of stratigraphy (Slatt and Abousleiman, 2011). Sierra et al. (2010) and Slatt and Abousleiman (2011) report that the degree of lamination plays a significant role in rock strength. Laboratory measurements concluded that core-plug-sized samples of laminated shale break more easily when stress is applied parallel and less easily when the stress is applied perpendicular to the lamination orientation (Slatt, 2011). The vertical histogram and BI calculation using elastic logs and the template in Figure 8c indicate a decrease in events toward the Forestburg Limestone, corresponding to an increase in clay minerals and ductility (Figure 11b). The decrease in microseismic events might be associated to the increase in interbedding in the top section of the Lower Barnett Shale, where we observe an increment in the clay content in these thin layers. As the clay content increases, it begins to support neighboring grains and impacts the velocities, creating a ductile zone in the reservoir.

To validate the brittle-ductile regions results, we extract the $\lambda\rho$ and $\mu\rho$ values at each microseismic event and plot them against our brittleness template. Note that most of the points fall into the area that we defined to be more brittle (Figure 12), validating our hypothesis

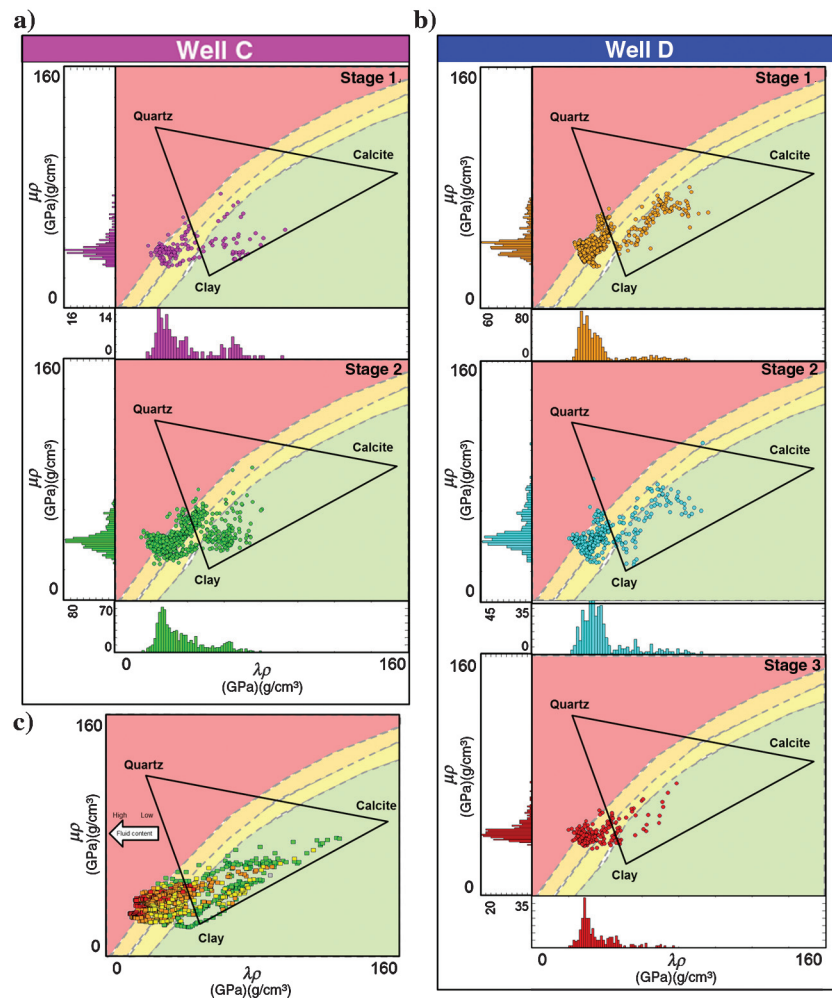
that the rock preferentially fractures in the more brittle regions.

Limitations

Shales are anisotropic. The BI to elastic parameters template is based on P- and S-wave sonic measurements carried out in vertical wells, which measures the vertical component of elastic impedance. The horizontal component of velocity (and hence impedance) is not measured at all. Surface seismic inversion is sensitive to vertical components of impedance at near angle incidence. Anisotropic effects influence reflections at larger angles of incidence. Although a more accurate BI to elastic parameters template should account for anisotropy, simple modeling experiments discussed in Perez (2011) show that ignoring anisotropy for a limited angle ($\theta < 30^\circ$) prestack impedance inversion is acceptable.

Furthermore, in this research, the ECS logs do not indicate any dolomite content in the seven wells, which disagrees with observations by Kale (2009), Karastathis (2007), and Singh (2008), with Singh (2008) reporting dolomitic mudstone lithofacies with 30%–40% of dolomite embedded in a clay matrix. Dennie (2010) and Dennie et al. (2012) find evidence of postdepositional

Figure 12. Extracted $\lambda\rho$ – $\mu\rho$ from each microseismic event location corresponding to (a) well C and (b) well D (well locations are shown in Figure 10c). (c) The $\lambda\rho$ – $\mu\rho$ cross-plot from the area around the well. Comparing the microseismic events distribution to those in panels (a and b) shows that most of microseismic events occurs in the area that we define as brittle (red) and less brittle (orange).



alteration in authigenic minerals, the carbonate minerals (e.g., calcite, dolomite, siderite, and ankerite) being the most common authigenic phases in the Barnett Shale. ECS and other standard mineralogy log tools are calibrated to detect the presence of silica (SiO_2), but they cannot deduce its origin. Using petrographic methods including secondary electron, backscattered electron, and cathodoluminescence imaging, Papazis and Milliken (2005) identify detrital and authigenic quartz in the Barnett Shale. Detrital quartz makes up to 40% of the quartz in the formation, and it occurs as silt-size grains and particles aggregated within the tests of agglutinated foraminifera. Also, authigenic quartz is found in veins, biologically derived replacements of skeletal debris (radiolaria), sealed fractures within individual detrital grains, and as cement within agglutinated foram tests (Papazis and Milliken, 2005).

Other studies have analyzed the relationship between brittleness and the mineralogical composition. In the case of the Austin chalk, the grain rimming versus pore filling correlates with different mechanical properties and natural fracture attributes, even though the modal composition is the same (Laubach et al., 2009).

The influence of kerogen in brittleness

The scanning electron microscopy (SEM) image from a Barnett Shale core (Figure 13) shows that the kerogen is located inside the grains in the sample, and it exhibits quasicircular pores (Sondergeld et al., 2010a). At a high pressure and temperature, we do not expect to find quasicircular pores. This circular structure suggests that the grains around the intragranular kerogen support the stress. In this example, a high TOC does not significantly imply high ductility and the kerogen does not affect the elastic properties of the rock. Slatt (2011) describes and classifies a variety of pore types that exist in the Barnett and the Woodford Shale, and Slatt and Abousleiman (2011) conclude that different pore types significantly influence the geomechanical properties.

Lucier et al. (2011) conclude that the gas saturation decreases the V_p/V_s ratio in unconventional shales, which leads to a lower Poisson's ratio calculation. The particularity about the Barnett Shale is that the kerogen is encapsulated in the pores of the rock, which does affect the mechanical properties of the rock. Given the granular support and the correlation of TOC with quartz in this study area, the effect of TOC is minimized such that high TOC rocks are “brittle” stratigraphically.

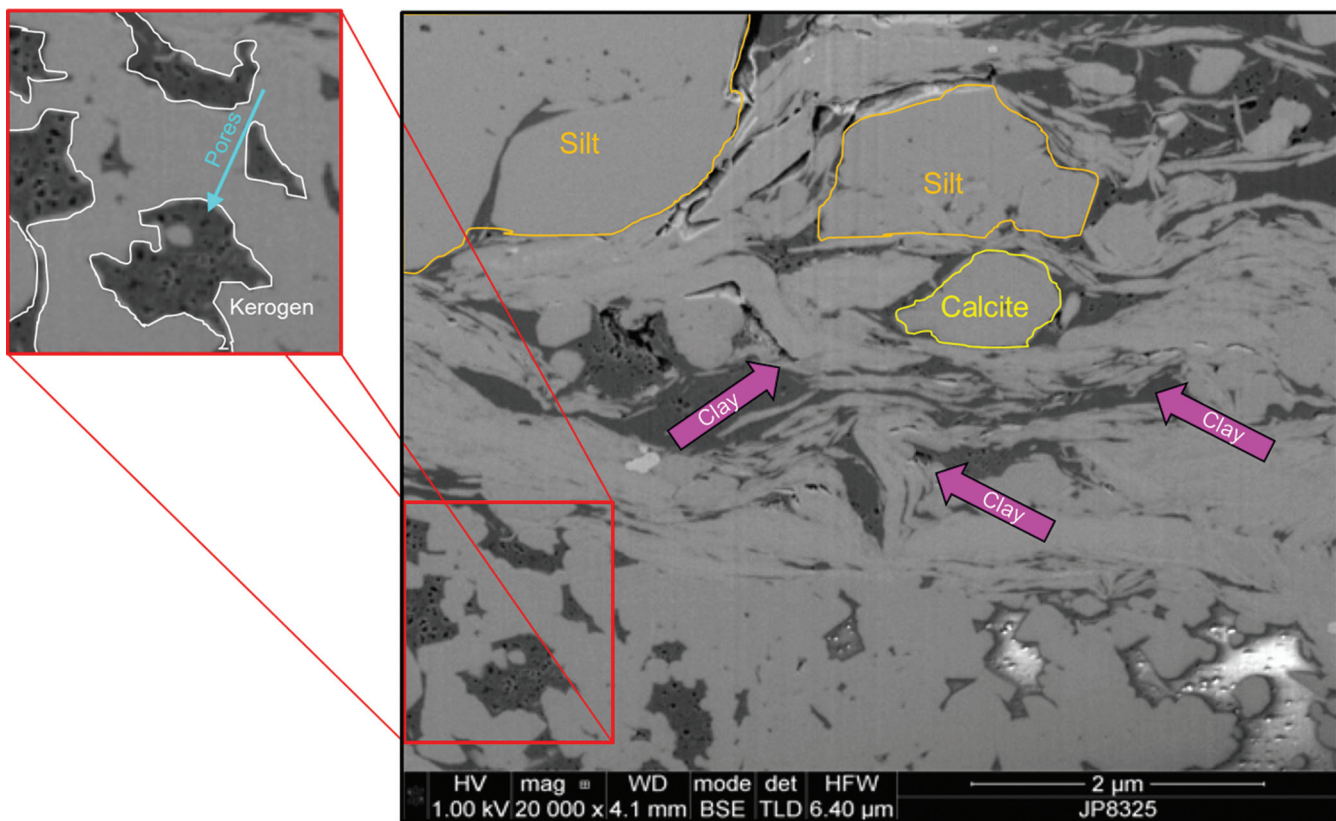


Figure 13. Backscattered SEM image of an ion-milled Barnett Shale sample imaged and ion milled in a dual-beam SEM (modified from Sondergeld et al. [2010a] and courtesy of OU MPGE Integrated Core Characterization Center). Larger silt (orange) and calcite (yellow) grains are mixed with clay (magenta) particles, and intragranular dark objects are interpreted as kerogen (white). The smaller circular darker objects within the kerogen are pores (cyan).

In this special case scenarios we found that those rocks that are more “frackable” are the ones that contain a higher amount of TOC.

Conclusions

The BI and brittleness average are commonly used to define brittleness in quartz-rich shales. In the case of the Barnett Shale, brittleness is dominated by quartz, whereas ductility is dominated by clay content and calcite. Although we anticipated that log and core description with the two more popular brittleness estimation techniques would show a consistent brittleness estimate, this was not the case. In particular, the brittleness average does not accurately predict the ductile behavior of limestones. We therefore modified a previous brittleness concept to construct a template based on mineralogy and elastic parameters measured in the study area. This template allows us to use a single brittleness for all lithologies in the target area: brittle shales, ductile shales, and ductile limestone fracture barriers.

Our template is validated through a suite of microseismic experiments, which shows most events occurring in brittle zones, fewer events in the ductile shale, and fewer events still in the limestone fracture barriers.

Acknowledgments

We would like to thank Devon Energy for providing the seismic and well data and for the financial support to complete this project, along with Schlumberger (Petrel) and CGG Veritas (Hampson-Russell) for providing the software licenses Petrel and Strata to the University of Oklahoma.

References

- Altindag, R., and A. Guney, 2010, Predicting the relationships between brittleness and mechanical properties (UCS, TS and SH) of rocks: Scientific Research and Essays, **5**, 2107–2118.
- Aubertin, M., and D. E. Gill, 1988, Une méthodologie d'évaluation du potentiel de coups de terrain dans les mines d'Abitibi: Colloque sur le Contrôle de Terrain (AMMQ), 47–77.
- Aubertin, M., D. E. Gill, and R. Simon, 1994, On the use of the brittleness index modified (BIM) to estimate the post-peak behaviour of rocks: in P. P. Nelson, and S. E. Laubach, eds., Proceedings of the 1st North American Rock Mechanics Symposium, AA Balkema, 945–952.
- Baron, L. I., 1992, Determination of properties of rocks: Gozgotekhizdat (in Russian).
- Berryman, J. G., P. A. Berge, and B. P. Bonner, 1999, Role of λ -diagrams in estimating porosity and saturation from seismic velocities: 69th Annual International Meeting, SEG, Expanded Abstracts, 176–179.
- Berryman, J. G., P. A. Berge, and B. P. Bonner, 2002, Estimating rock porosity and fluid saturation using only seismic velocities: Geophysics, **67**, 391–404, doi: [10.1190/1.1468599](https://doi.org/10.1190/1.1468599).
- Bowker, K. A., 2003, Recent developments of the Barnett Shale play, Fort Worth Basin: West Texas Geological Society Bulletin, **42**, 4–11.
- Browning, D. B., 2006, Investigating correlations between microseismic event data, seismic curvature, velocity anisotropy, and well production in the Barnett Shale, Fort Worth Basin, Texas: Master's thesis, The University of Oklahoma.
- Bustin, M. R., 2006, Geology report: Where are the high-potential regions expected to be in Canada and the US? Capturing opportunities in Canadian shale gas: Presented at The Canadian Institute's 2nd Annual Shale-Gas Conference.
- Coates, D. F., and R. C. Parsons, 1966, Experimental criteria for classification of rock substances: International Journal of Rock Mechanics and Mining Sciences and Geomechanics Abstracts, **3**, 181–189, doi: [10.1016/0148-9062\(66\)90022-2](https://doi.org/10.1016/0148-9062(66)90022-2).
- Daugherty, J., and T. Urbancic, 2009, Microseismic monitoring of a carbon sequestration field test: Frontiers and innovation: Presented at Frontiers + Innovation — CSPG CSEG CWLS Convention.
- Davis, D., and S. J. Reynolds, 1996, Structural geology of rocks and regions, 2nd ed.: Wiley.
- Deacon, R. J., 2011, Barnett provides future returns: E&P Magazine, **2011**, 71–75.
- Dennie, D., R. D. Elmore, J. Deng, E. Manning, and J. Pananalal, 2012, Paleomagnetism of the Mississippian Barnett Shale, Fort Worth Basin, Texas: Journal of the Geological Society, London, **371**, 89–106, doi: [10.1144/SP371.10](https://doi.org/10.1144/SP371.10).
- Dennie, D. P., 2010, An integrated paleomagnetic and diagenetic investigation of the Barnett Shale and underlying Ellenburger Group carbonates, Fort Worth Basin, Texas: Ph.D. dissertation, ConocoPhillips School of Geology and Geophysics.
- Ellis, M. A., S. E. Laubach, P. Eichhubl, J. E. Olson, and P. Hargrove, 2012, Fracture development and diagenesis of Torridon Group Applecross Formation, near An Teallach, NW Scotland: Millennia of brittle deformation resilience?: Journal of the Geological Society, London, **169**, 297–310, doi: [10.1144/0016-76492011-086](https://doi.org/10.1144/0016-76492011-086).
- Gale, J. F., R. M. Reed, and J. Holder, 2007, Natural fractures in the Barnett Shale and their importance for hydraulic fracture treatments: AAPG Bulletin, **91**, 603–622, doi: [10.1306/11010606061](https://doi.org/10.1306/11010606061).
- Gao, C., 2011, Multiscale ensemble Kalman filter for history matching and characterization of Barnett Shale: M.S. thesis, Mewbourne School of Petroleum and Geological Engineering: The University of Oklahoma.
- Goodway, B., T. Chen, and J. Downton, 1997, Improved AVO fluid detection and lithology discrimination using Lamé parameters $\lambda\rho$, $\mu\rho$ and $\frac{\lambda}{\mu}$ fluid stack from P- and S-inversion: 67th Annual International Meeting, SEG, Expanded Abstracts, 183–186.

- Goodway, B., M. Perez, J. Varsek, and C. Abaco, 2010, Seismic petrophysics and isotropic-anisotropic AVO methods for unconventional gas exploration: The Leading Edge, **29**, 936–944.
- Goodway, B., J. Varsek, and C. Abaco, 2006, Practical applications of P-wave AVO for unconventional gas resource plays — I: Seismic petrophysics and isotropic AVO: CSEG Recorder, **31**, 90–95.
- Grieser, B., and J. Bray, 2007, Identification of production potential in unconventional reservoirs: Presented at SPE Production and Operations Symposium.
- Hajibabdolmajid, V., and P. Kaiser, 2003, Brittleness of rock and stability assessment in hard rock tunneling: Tunneling and Underground Space Technology, **18**, 35–48, doi: [10.1016/S0886-7798\(02\)00100-1](https://doi.org/10.1016/S0886-7798(02)00100-1).
- Handin, J., and R. V. Hager, 1957, Experimental deformation of sedimentary rocks under confining pressure: Tests at room temperature on dry samples: AAPG Bulletin, **41**, 1–50.
- Handin, J., and R. V. Hager, 1958, Experimental deformation of sedimentary rocks under confining pressure: Tests at high temperature on dry samples: AAPG Bulletin, **42**, 2892–2934.
- Handin, J., R. V. Hager, M. Friedman, and J. N. Feather, 1963, Experimental deformation of sedimentary rocks under confining pressure: Pore pressure tests: AAPG Bulletin, **47**, 717–755.
- Heidbach, O., M. Tingay, A. Barth, J. Reinecker, D. Kurfe, and B. Muller, 2009, The world stress map based on the database release 2008, equatorial scale 1:46,000,000: Commission for the Geological Map of World.
- Hetenyi, M., 1966, Handbook of experimental stress analysis: Wiley.
- Jarvie, D. M., 2003, Evaluation of unconventional natural gas prospects: The Barnett Shale fractured shale gas model: Presented at 21st International Meeting on Organic Geochemistry.
- Jarvie, D. M., R. J. Hill, T. E. Ruble, and R. M. Pollastro, 2007, Unconventional shale-gas systems: The Mississippian Barnett Shale of North-Central Texas as one model for thermogenic shale-gas assessment: AAPG Bulletin, **91**, 475–499, doi: [10.1306/12190606068](https://doi.org/10.1306/12190606068).
- Kale, S., 2009, Petrophysical characterization of Barnett Shale play: M.S. thesis, Mewbourne School of Petroleum and Geological Engineering: The University of Oklahoma.
- Karastathis, A., 2007, Petrophysical measurements on tight gas shale: M.S. thesis, Mewbourne School of Petroleum and Geological Engineering: The University of Oklahoma.
- Laubach, S. E., J. E. Olson, and M. R. Gross, 2009, Mechanical and fracture stratigraphy: AAPG Bulletin, **93**, 1413–1426, doi: [10.1306/07270909094](https://doi.org/10.1306/07270909094).
- Loucks, R. G., 2008, Origin and modification of Lower Ordovician Ellenburger Group paleokarst breccias and fractures in Central and West Texas, in I. D. Sasowsky, C. T. Feazel, J. E. Mylroie, A. N. Palmer, and M. V. Palmer, eds., Karst from recent to reservoirs: Karst Waters Institute, Special Publication, vol. 14, 130–135.
- Lucier, A., R. Hofmann, and L. Bryndzia, 2011, Evaluation of variable gas saturation on acoustic log data from the Haynesville Shale gas play, NW Louisiana, USA: The Leading Edge, **30**, 300–311, doi: [10.1190/1.3567261](https://doi.org/10.1190/1.3567261).
- Mavko, G., T. Mukerji, and J. Dvorkin, 2009, The rock physics handbook: Cambridge University Press.
- McGillivray, P., 2005, Microseismic and time-lapse seismic monitoring of a heavy oil extraction process at Peace River, Canada: CSEG Recorder, **5**, 5–9.
- Montgomery, S. L., 2005, Mississippian Barnett Shale, Fort Worth Basin, North-Central Texas: Gas-shale play with multi-trillion cubic foot potential: AAPG Bulletin, **89**, 155–175, doi: [10.1306/09170404042](https://doi.org/10.1306/09170404042).
- Noe, J., 2011, Microseismic frac mapping: Moving beyond the dots from an engineering perspective: Presented at OGS Shales Moving Forward Workshop, Oklahoma Geological Society.
- Obert, L., and W. I. Duvall, 1967, Rock mechanics and the design of structures in rock: Wiley.
- Papazis, P. K., and K. Milliken, 2005, Cathodoluminescent textures and the origin of quartz in the Mississippian Barnett Shale, Fort Worth Basin, Texas: Presented at the AAPG Annual Convention and Exhibition.
- Perez, M., 2011, Developing templates for integrating quantitative geophysics and hydraulic fracture completions data: Part I — Principles and theory: 81st Annual International Meeting, SEG, Expanded Abstracts, 1794–1798.
- Perez, R., 2009, Quantitative analysis of gamma ray parasequences in the Barnett Shale: M.S. thesis, ConocoPhillips School of Geology and Geophysics: The University of Oklahoma.
- Ramsey, J. G., 1967, Folding and fracturing of rocks: McGraw-Hill.
- Refunjol, X. E., 2010, Hydraulically-induced microseismic fracture characterization from surface seismic attributes and seismic inversion: A North Texas Barnett Shale case of study: M.S. thesis, ConocoPhillips School of Geology and Geophysics.
- Refunjol, X. E., K. M. Keranen, J. H. LeCalvez, and K. J. Marfurt, 2012, Integration of hydraulically induced microseismic events location with active seismic attributes: A North Texas Barnett Shale case of study: Geophysics, **77**, no. 3, KS1–KS12, doi: [10.1190/geo2011-0032.1](https://doi.org/10.1190/geo2011-0032.1).
- Ribacchi, R., 2000, Mechanical tests on pervasively jointed rock material: Insight into rock mass behaviour: Rock Mechanics and Rock Engineering, **33**, 243–266, doi: [10.1007/s006030070002](https://doi.org/10.1007/s006030070002).
- Rickman, R., M. Mullen, E. Petre, B. Grieser, and D. Kundert, 2008, A practical use of shale petrophysics for stimulation design optimization: All shale plays are not clones of the Barnett Shale: Presented at SPE Annual Technical Conference and Exhibition.

- Saldungaray, P., and T. Palish, 2012, Hydraulic fracture optimization in unconventional reservoirs: *World Oil*, **233**.
- Schmoker, J. W., 1981a, Organic content of Devonian shale in western Appalachian Basin: *AAPG Bulletin*, **64**, 2156–2165.
- Schmoker, J. W., 1981b, Determination of organic matter content of Appalachian Devonian shales from gamma-ray logs: *AAPG Bulletin*, **65**, 1285–1298.
- Sierra, R., M. H. Tran, Y. N. Abousleiman, and R. M. Slatt, 2010, Woodford Shale mechanical properties and impacts of lithofacies: Presented at 44th U.S. Rock Mechanics Symposium and 5th U.S.–Canada Rock Mechanics Symposium, ARMA10-461.
- Simon, Y., 2005, Stress and fracture characterization in a shale reservoir, North Texas, using correlation between new seismic attributes and well data: M.S. thesis, Department of Geosciences, University of Houston.
- Singh, P., 2008, Lithofacies and sequence stratigraphic framework of the Barnett Shale: Ph.D. dissertation, ConocoPhillips School of Geology and Geophysics: The University of Oklahoma.
- Slatt, R. M., 2011, Important geological properties of unconventional resource shales: *Central European Journal of Geoscience*, **3**, 435–448, doi: [10.2478/s13533-011-0042-2](https://doi.org/10.2478/s13533-011-0042-2).
- Slatt, R. M., and Y. N. Abousleiman, 2011, Merging sequence stratigraphy and geomechanics for unconventional gas shales: *The Leading Edge*, **30**, 274–282, doi: [10.1190/1.3567258](https://doi.org/10.1190/1.3567258).
- Slatt, R. M., and N. R. O'Brien, 2011, Pore types in the Barnett and Woodford gas shales: Contribution to understanding gas storage and migration pathways in fine-grained rocks: *AAPG Bulletin*, **95**, 2017–2030, doi: [10.1306/03301110145](https://doi.org/10.1306/03301110145).
- Sondergeld, C. H., R. J. Ambrose, C. S. Rai, and J. Moncrieff, 2010a, Micro-structural studies of gas shales: Presented at SPE Unconventional Gas Conference.
- Sondergeld, C. H., K. E. Newsham, J. T. Cominsky, M. C. Rice, and C. S. Rai, 2010b, Petrophysical considerations in evaluating and producing shale gas resources: Presented at SPE Unconventional Gas Conference.
- Thompson, A. M., 2010, Induced fracture detection in the Barnett Shale, Fort Worth Basin, Texas: M.S. thesis, ConocoPhillips School of Geology and Geophysics.
- Thomsen, L., 1986, Weak elastic anisotropy: *Geophysics*, **51**, 1954–1966, doi: [10.1190/1.1442051](https://doi.org/10.1190/1.1442051).
- Walper, J. L., 1982, Plate tectonic evolution of the Fort Worth Basin: Dallas Geological Society.
- Wang, F. P., and J. F. W. Gale, 2009, Screening criteria for shale-gas systems: *Gulf Coast Association of Geological Societies Transactions*, **59**, 779–793.
- Waters, G., H. Ramakrishnan, J. Daniels, D. Bently, J. Belhadi, and D. Sparkman, 2009, Utilization of real time microseismic monitoring and hydraulic fracture diversion technology in the completion of Barnett Shale horizontal wells: Presented at OTC.
- Wells, F., 2004, A new method to help identify unconventional targets for exploration and development through integrative analysis of clastic rock properties: *Houston Geological Society Bulletin*, **47**, 34–49.
- Zhang, K., 2010, Seismic attribute analysis of unconventional reservoirs, and stratigraphic patterns: Ph.D. dissertation, ConocoPhillips School of Geology and Geophysics: The University of Oklahoma.



Roderick Perez is currently working as a technical service consultant for DrillingInfo — Transform Software and Services, Inc., in Houston, Texas. Born in Caracas, Venezuela, he completed his undergraduate degree in geophysics engineering at the Universidad Simon Bolivar (Caracas, Venezuela) in 2007, after spending a year as an exchange student at the University of Oklahoma (OU) during the fall of 2005 to the spring of 2006. He completed his M.S. in geology at OU in 2008 under the direction of Dr. Slatt, and he completed his Ph.D. in geophysics under the guidance of Dr. Marfurt in 2013. His dissertation research focuses on seismic attributes applied to reservoir characterization of unconventional reservoirs, with results additionally calibrated with available microseismic data. He has authored several articles with his two advisors, and his dissertation is under review for publication as a book. He has also reviewed several papers for *Interpretation*, among other geoscience magazines. As part of a group effort, He won first place in the 2008 AAPG Imperial Barrel Award (IBA) competition along with his four teammates representing the OU. He also was the recipient of the SEG Scholar—Charles C. McBurney Memorial Award 2010–2011, among other scholarships. In addition to his academic duties as a full-time research assistant at OU, he participated and accepted leadership roles in several extracurricular activities on campus, such as president of the OU-SEG student chapter (2009–2010), vice-president (2007–2008), and secretary (2006–2007) of the Association Friends of Venezuela. He is the IBA—Latin America Coordinator for Venezuela, Mexico, and Trinidad and Tobago, and he participates in several committees in AAPG and SEG. He continues to stay informed on advancements in the oil and gas community and always looks forward to learning about new data sets and finding new ways to provide value back value back to companies with which he collaborates.



Kurt Marfurt began his geophysical career as an assistant professor teaching mining geophysics at Columbia University's Henry Krumb School of Mines in New York. After five years, he joined Amoco at its Tulsa Research Center. Through successive reorganizations at Amoco, Marfurt obtained diverse experience in seismic modeling, migration, signal analysis, basin analysis, seismic-attribute analysis, and multicomponent analysis. Through

Amoco, he won five patents, two in seismic coherence technology. Marfurt joined the University of Houston in 1999 as a professor in the Department of Geosciences and as director of the Center for Applied Geosciences and Energy, where his primary emphasis is on development and calibration of new seismic-attribute technology.

Marfurt joined the University of Oklahoma as the Frank and Henrietta Schultz Chair and Professor of Geophysics. His recent work has focused on applying coherence, spectral decomposition, structure-oriented filtering, and volumetric curvature to mapping fractures and karst as well as attribute-assisted processing.